LAWRENCE
LIVERMORE
NATIONAL
LABORATORY

UCRL-JRNL-229616

A model for plasticity kinetics and its role in simulating the dynamic behavior of Fe at high strain rates

J. D. Colvin, R. W. Minich, D. H. Kalantar

April 2, 2007

International Journal of Plasticity

Updated October 14, 2003

Submitted to International Journal of Plasticity, March 30, 2007
Revised manuscript submitted November 1, 2007: UCRL-JRNL-229616

A model for plasticity kinetics and its role in simulating the dynamic behavior of Fe at high strain rates

Jeffrey D. Colvin*, Roger W. Minich, and Daniel H. Kalantar
Lawrence Livermore National Laboratory, P.O. Box 808, Livermore, CA 94551 USA

Abstract

The recent diagnostic capability of the Omega laser to study solid-solid phase transitions at pressures greater than 10 GPa and at strain rates exceeding 10^7 s^{-1} has also provided valuable information on the dynamic elastic-plastic behavior of materials. We have found, for example, that plasticity kinetics modifies the effective loading and thermodynamic paths of the material. In this paper we derive a kinetics equation for the time-dependent plastic response of the material to dynamic loading, and describe the model's implementation in a radiation-hydrodynamics computer code. This model for plasticity kinetics incorporates the Gilman model for dislocation multiplication and saturation. We discuss the application of this model to the simulation of experimental velocity interferometry data for experiments on Omega in which Fe was shock compressed to pressures beyond the α-to-ε phase transition pressure. The kinetics model is shown to fit the data reasonably well in this high strain rate regime and further allows quantification of the relative contributions of dislocation multiplication and drag. The sensitivity of the observed signatures to the kinetics model parameters is presented.

Keywords: dynamics (A); shock waves (A); crystal plasticity (B); rate-dependent material (B).

* Corresponding author. Tel.: (925) 422-3273; FAX: (925) 424-4737; email: colvin5@llnl.gov

1. Introduction

For several years now, high-power lasers have been used to explore high strain-rate materials dynamics (Remington *et al*., 2004). Materials dynamics experiments have been conducted at several laser facilities that are capable of shock-compressing solids at pressures greater than 10 GPa and at strain rates exceeding 10^7 s^{-1}. In this paper we present an analysis of materials dynamics experiments conducted at the Omega Laser (Boehly *et al*., 1995) at the University of Rochester, Rochester, New York.

In recent experiments at Omega, Kalantar *et al*. (2005) observed the α-to-ε solid-solid phase transition in single-crystal Fe. In these experiments they made use of a newly developed multi-film-plane detector (Kalantar *et al*., 2003) to record dynamic diffraction from multiple lattice planes simultaneously. The detector is large compared to the sample and is placed so that it can record Bragg diffraction from many lattice planes at a range of angles. The shock was created in the Fe sample by using one laser beam to directly illuminate the target at intensities of $2\text{x}10^{10}$ – 10^{12} W/cm^2. The target consisted of the thick (200-250 μm) Fe sample overlain by a thin (15 μm) parylene (C_8H_8) ablator so as to keep the laser beam from directly heating the Fe; a flash coating of Al on the parylene served as a shine-through barrier. See Fig. 1a. A separate laser beam illuminated an Fe backlighter foil, creating the 6.7 keV Fe K-shell x-rays that served as the Bragg diffraction probe beam. These backlighter x-rays were diffracted from multiple lattice planes on the front (drive) side of the shocked Fe. More details of the experiment are given by Kalantar *et al*. (2005), and more details of the diffraction analysis are given by Hawreliak *et al*. (2006).

Quantitative interpretation of the diffraction results depends on knowing the pressure applied by the laser drive at the front surface of the Fe, the side illuminated by the laser. There is no way to measure the pressure directly on the front side. Instead, a VISAR velocity interferometer (Barker and Hollenbach, 1972) was used to measure the free-surface velocity of the Fe (i.e., the velocity on the back or undriven side of the Fe).

The front-surface conditions are then related to the free-surface conditions via propagation of the elastic and plastic waves through the Fe from front to back, given the equation of state (EOS) of the Fe. In practice, what we do is a complete simulation of the response of the material using the 2D radiation-hydrodynamics code LASNEX (Zimmerman and Kruer, 1975). Hydrodynamics is treated in a Lagrangian formulation, with the elastic-plastic equations differenced on a staggered mesh (cell-centered stresses and strains, node-centered forces and velocities) by means of classical finite-difference techniques. The EOS is the analytical Quotidian EOS (More *et al*., 1988), which reduces to a Gruneisen EOS at low temperatures, in which the ratio of the thermal pressure to the thermal energy is a constant (Zel'dovich and Raizer, 2002). We use a single-phase EOS which does not account for the entropy change at the α–ε phase

boundary. For our purposes here, though, a single-phase EOS is adequate since the Fe gets above the phase transition pressure in only some of the shots, and then only in the first few microns and for a short time. Radiation transport is calculated by multi-group diffusion, with opacities calculated from the average atom model. Cold opacities in the parylene ablator are used to model propagation of the Al K-shell x-rays (created by the interaction of the laser light directly with the Al shine-through barrier on the surface of the target) that preheat the Fe (Colvin and Kalantar, 2006). The laser beam propagation is followed by a 3D ray tracing algorithm, with absorption by inverse bremsstrahlung. Full transport physics is included, with metallic conductivities in the Fe.

The main purpose of the simulations is to determine the pressure drive history at the front surface of the Fe, given the measured laser power history. We benchmark the simulation by matching the simulated velocity history at the free surface with the one measured by VISAR. As shown in Fig. 1b, we can match both the velocity amplitude of the elastic wave and the velocity amplitude of the plastic wave with the simulations (Colvin and Kalantar, 2006). However, we do not match the time history. In particular, we see in the VISAR traces the distinct signature of plasticity kinetics effects: the shear stress overshoots the equilibrium value of the flow stress and then relaxes back, delaying the onset of fully plastic flow. This behavior, of course, is not captured at all in a simulation in which the material is assumed to transition to perfectly plastic flow instantaneously when the shear stress reaches the equilibrium flow stress.

We see this characteristic signature of kinetics effects in all the VISAR data from these laser-driven materials dynamics experiments. We are confident that we have the peak pressure at the front surface correct since we can match the peak velocity at the back surface. Thus, these VISAR data --- even though somewhat noisy because of unavoidable intensity fluctuations in the drive laser --- can be used to indicate the plasticity kinetics processes that modify the temporal shape of the pressure wave during its propagation through the target. The purpose of the work reported in this paper is to describe a plasticity kinetics model that, when incorporated into these LASNEX simulations, provides a much better match to these VISAR data.

In the next Section we derive a kinetics equation for the plastic flow, based on a model for dislocation multiplication and saturation first given by Gilman (1965). We also discuss how the kinetics model was implemented in the hydrodynamics code. In Section 3 we discuss the simulation of the Fe VISAR data with plasticity kinetics, and the sensitivity of the fit to variations in the model parameters. Concluding remarks and a summary are in Section 4.

2. A plasticity kinetics model

2.1 Derivation of the kinetics equation

It is important to understand at the outset that our treatment of time-dependent plasticity is different than most past treatments in that it is not a model for visco-plasticity. In visco-plastic deformation, the shear stress is directly proportional to the plastic strain rate, such as in a Newtonian (constant viscosity) fluid, so the shear stress (analogously, the drag force in a Newtonian fluid) relaxes to zero as a result of the plastic deformation. There has been a lot of work on developing models for the kinetics of visco-plasticity (see, for example, Magnenet *et al*., 2007), and even a model that treats perfect plasticity as visco-plasticity (Colvin *et al*., 2003). The model we present here, on the other hand, is for time-dependent perfect plasticity, i.e., where the shear stress relaxes to a constant non-zero value as a result of the plastic deformation.

We start with Hooke's Law:

$$\mathbf{s}_{ij} = 2G\varepsilon_{ij} \tag{1}$$

where the $\mathbf{s}_{ij}$ are the deviatoric stresses, $\boldsymbol{\varepsilon}_{ij}$ the elastic strains, and G the shear modulus. We differentiate equation (1) and then write the differential equation as a difference equation, obtaining:

$$\mathbf{s}_{ij}' = \mathbf{s}_{ij} + 2G\dot{\varepsilon}_{ij}\delta t\ , \tag{2}$$

where δt is the differential time step, the dot over a symbol indicates a time derivative, and the prime indicates the variable at time $t+\delta t$. Then, we write the elastic strain as the difference between the total strain θ_{ij} and the plastic strain ε_{ij}^{p}:

$$\mathbf{s}_{ij}' = \mathbf{s}_{ij} + 2G[\dot{\theta}_{ij} - \dot{\varepsilon}_{ij}^{p}]\delta t\ . \tag{3}$$

Now, from the von Mises condition for plasticity, i.e.,

$$\begin{aligned} &\mathbf{s}_{ij}\mathbf{s}_{ij} = \frac{2}{3}Y^2; \\ &\dot{\varepsilon}_p = \sqrt{(2/3)\dot{\varepsilon}_{ij}^{p}\dot{\varepsilon}_{ij}^{p}} \end{aligned} \tag{4}$$

we can re-write equation (3) as

$$\mathbf{s}_{ij}' = \mathbf{s}_{ij} + \{2G\dot{\theta}_{ij} - \frac{3G}{Y}\mathbf{s}_{ij}'\dot{\varepsilon}_p'\}\delta t\ , \tag{5}$$

with Y the yield strength of the material.

Following Steinberg and Lund (1989) we note that the first two terms on the right-hand side of equation (6) do not depend on the plastic strain rate, and hence we define a new variable $\hat{\mathbf{s}}_{ij}$ that is the sum of these two terms. Thus, at each time step δt in the calculation, the shear stress is relaxed by a factor that depends on the plastic strain rate; i.e.,

$$\mathbf{s}'_{ij} = \frac{\hat{\mathbf{s}}_{ij}}{1+\frac{3G}{\tau}\dot{\varepsilon}'_p \delta t}, \tag{6}$$

with τ the flow stress at time step δt.

We now specify the time-dependent plastic strain rate by adapting the Gilman (1965) model of dislocation multiplication and saturation. Gilman's key insight is that the dislocation density ρ does not stay constant during plastic deformation. Thus, we start with Orowan's equation and account for the time variation of the dislocation density, so the plastic strain and plastic strain rate are:

$$\begin{aligned} \varepsilon_p &= bl\rho, \\ \dot{\varepsilon}_p &= bv_0\rho + bl\frac{d\rho}{dt} \end{aligned} \tag{7}$$

where b is the Burger's vector, l is a characteristic length scale for the dislocation motion and v_0 the dislocation velocity.

Dislocation density grows by multiplication, which is proportional to the dislocation density, and saturates by drag and annihilation. The annihilation is largely by binary coalescence, which is proportional to the square of the dislocation density. Thus, we can write the time rate of change of the dislocation density as

$$d\rho/dt = \alpha\rho - \beta\rho^2, \tag{8}$$

with α and β constants. Integrating equation (9) we get

$$\rho = \frac{\alpha\rho_0 e^{\alpha t}}{[\alpha + \beta\rho_0(e^{\alpha t} - 1)]}. \tag{9}$$

Gilman starts with equation (9) substituted into the second of equations (7), and then modifies it by accounting for the dislocation drag stress D and hardening stress H to write the plastic strain rate as a function of the variable plastic strain and the variable flow stress, τ:

$$\dot{\varepsilon}_p = bv_0(\rho_0 + M\varepsilon_p)\exp\{-(D + H\varepsilon_p)/\tau\}. \quad (10)$$

The initial dislocation density is ρ_0 and M is the dislocation density multiplication coefficient.

It is relatively straight-forward to find from equation (10) that the plastic strain rate is a maximum at plastic strain $\varepsilon_p = \tau/H$ for the usual case of M >> ρ_0.

We then have the following picture of time-dependent plastic deformation. The material initially compresses elastically along the shock compression direction under uni-axial shock compression. Then, when the deviatoric stress reaches the von Mises yield condition, the flow stress initially overshoots its equilibrium value (the yield stress) as the plastic strain and plastic strain rate increase. The plastic strain rate reaches a maximum value, and then the plastic strain rate decreases again as the flow stress relaxes back to its equilibrium value, as illustrated schematically in Fig. 2.

Our particular contribution --- in addition to the recognition that dislocation multiplication is the key to modeling plasticity kinetics --- is to combine the Steinberg and Lund (1989) formulation with the Gilman (1965) model to derive a plasticity kinetics equation that can be incorporated relatively easily into a hydrodynamics code. Thus, we can write a kinetics equation, following the logic with which we arrived at equation (6), as

$$f(\tau) = 3G\dot{\varepsilon}_p\delta t + \tau - [\frac{3}{2}\mathbf{s}_{ij} \bullet \mathbf{s}_{ij}]^{1/2} = 0, \quad (11)$$

with $\dot{\varepsilon}_p$ given by equation (10).

2.2 Implementation of the model in the hydrodynamics code

The first two terms in the kinetics equation, equation (12), both contain the flow stress, τ. We solve for the flow stress as the root of the kinetics equation, $f(\tau) = 0$. We find the root via a Newton-Raphson iteration. Thus, at each time t_m, we find the flow stress τ by iterating the kinetics equation:

$$\tau_{n+1} = \tau_n - \frac{f(\tau_n)}{df(\tau_n)/d\tau}. \quad (12)$$

The iteration is continued until the difference between the flow stresses on successive steps in the iteration, $\tau_{n+1} - \tau_n$, is less than some pre-set convergence criterion. Then, $\dot{\varepsilon}_p$ is updated at time t_m with the new τ and the plastic strain is updated as:

$$\varepsilon_p(t_m) = \varepsilon_p(t_{m-1}) + \dot{\varepsilon}_p(t_m)\delta t_m. \tag{13}$$

Finally, we decrease the deviatoric stress via equation (6). We continue this prescription at each time step until the deviatoric stress relaxes back to its equilibrium value.

In the 2D hydrodynamics code, the hydrodynamic equations --- conservation of mass, momentum, and energy --- are written in cylindrical co-ordinates, so

$$|\mathbf{s}\bullet\mathbf{s}| = 2(s_{rr}^2 + s_{zz}^2 + s_{rz}^2 + s_{zz}s_{rr}), \tag{14}$$

which for uni-axial compression along the z-axis reduces to

$$|\mathbf{s}\bullet\mathbf{s}| = (3/2)s_{zz}^2. \tag{15}$$

Thus, the von Mises criterion for the onset of plastic flow, the first of equations (4), becomes

$$|s_{zz}| = (2/3)Y_0, \tag{16}$$

where Y_0 is the equilibrium yield strength.

In addition to the four parameters of the kinetics model that need to be specified --- initial dislocation density ρ_0, dislocation multiplication coefficient M, dislocation drag stress D, and hardening stress H --- we also need to specify Y_0.

3. Modeling the laser-driven Fe experiments

In these particular experiments the pulse duration, 6 ns, was very short compared to the transit time of the pressure pulse in the Fe foil. Because of this, a rarefaction wave overtakes the propagating pressure pulse after the laser turns off, reducing the peak pressure and broadening its spatial profile as the wave propagates to the back of the foil, as shown in Fig. 3. Since the peak overshoot shear stress for this loading pressure profile does not necessarily exceed the von Mises criterion everywhere in the Fe, one single choice for Y_0 in the modeling does not provide a perfect fit to the entire temporal profile of the measured free-surface velocity history.

Nonetheless, the model provides a qualitatively improved temporal fit to the data, as shown in Fig. 4. Here we show, in panels a and b of Fig. 4, two model fits to the Visar data from one of the Omega shots in which 117 J of 1/3 μm laser light was incident on a target containing a 250-μm-thick single-crystal Fe foil, with the normal to the foil oriented in the <001> crystallographic direction. This is the

direction of the shock propagation. In Fig. 4a we show the model fit (the red curve) for a single choice of Y_0 = 1.2 GPa for the entire foil. The blue curve shows the simulated velocity history without plasticity kinetics, with Y_0 = 3.6 GPa. All the model parameters for the simulation with kinetics are shown in the second column of Table 1. In this simulation, the kinetics model is turned on when the deviatoric stress reaches the von Mises condition for a yield strength of $3Y_0$, and allows it to relax back to a flow stress corresponding to Y_0. For this choice of Y_0, most of the zones in the back 20 μm of the foil never get to a deviatoric stress that exceeds the von Mises criterion, so the plasticity kinetics never turns on; i.e., the back 20 μm or so of the foil deforms only elastically. This artificial discontinuity in the material response possibly explains the anomalous "plateau" features in the simulated velocity history shown in Fig. 4a between 44 and 46 ns and between 47 and 49 ns.

The later (47-49 ns) plateau is reduced using a lower value of Y_0 = 0.25 GPa in the back 20 μm of the foil, forcing the plasticity kinetics to turn on everywhere, as shown in the red curve in Fig. 4b. All the model parameters for this simulation are shown in the third column of Table 1. In this simulation, the kinetics model is turned on when the deviatoric stress reaches the von Mises condition for a yield strength of $2Y_0$, and allows it to relax back to a flow stress corresponding to Y_0. As seen in Fig. 4b, there are still anomalous discontinuities in the simulated velocity history; these are numerical artifacts that result from the artificial discontinuities in Y_0 in the model.

We also used the model to simulate a higher-energy laser shot. In this shot, 179 J of 1/3 μm laser light was incident on a target containing a 200-μm-thick single-crystal Fe foil, with the normal to the foil again oriented in the <001> crystallographic direction. In Fig. 4c we show the model fit (the red curve again) for a single choice of Y_0 = 1.0 GPa for the entire foil, again turning on the kinetics when the deviatoric stress reaches the von Mises condition for a yield strength of $2Y_0$. All the model parameters for this simulation are shown in the fourth column of Table 1. In this case, with the higher energy and hence higher pressure drive, and with the 20% thinner foil, we can get by with a single value for Y_0 throughout the foil to get a fit with fewer discontinuities than for the thicker foil. As for the 117 J shot, the simulation without kinetics (the blue curve) was done with Y_0 = 3.6 GPa.

4. Summary and concluding remarks

We have also recorded Visar data for Fe <111>, showing peak velocity at elastic wave break-out of 0.15 μm/ns (compared to the 0.20 – 0.25 μm/ns for the Fe <001>), and which require different "best fit" model parameters. The rate of decay of the elastic precursor depends on the Gilman model parameters, as expected. Of the four Gilman model parameters, the fit is most sensitive to the

dislocation multiplication coefficient, M --- which sets the initial rise to peak --- and the dislocation drag stress, D --- which sets the time over which the plastic wave develops. It is of interest to note that the parameter values for the high strain rates for Fe in the present study are comparable to the values for modeling Fe at the lower strain rates typical of gas gun experiments and for modeling the precursor decay as observed by Taylor and Rice (1963), but we have not yet examined this issue in detail. Overall, though, the simulated free-surface velocity history is relatively insensitive to variations in the four parameters of the Gilman equation, ρ_0, M, D, and H. The results are much more sensitive to the choice of Y_0, which defines when the model turns on and when it turns off in each zone.

We find a similar sensitivity to Y_0 in our modeling of more recent VISAR data from laser-driven isentropic compression experiments (Smith et al. 2006) on much thinner metal foils in which the pressure varies little from front to back. This finding suggests that the Y_0 sensitivity is not a result of the loading history, but is likely the result of some artifact in the model and/or in its implementation in the code. The final form of the model and its implementation are a work in progress.

Nonetheless, we have shown that a consideration of plasticity kinetics effects is crucial to data interpretation; without this consideration we simply cannot explain the behavior of materials compressed at high strain rates. We chose the Gilman model as the initial candidate to model plasticity kinetics effects because it is the only model to account for dislocation multiplication in these high strain rate regimes.

Finally, we find that accounting for the kinetics of the plasticity in the simulations reduces the calculated peak hydrostatic pressure at the front of the Fe (where the diffraction data is taken) by ~20%, as shown in Fig. 5. The temperature on release is lower, too. Thus, the plasticity kinetics modifies both the hydrodynamic path and the thermodynamic path followed by the shock-compressed material.

In summary, we find that:

- Quantitative interpretation of the diffraction data from the laser-driven Fe experiments relies on knowing accurately the pressure history at the front (drive) surface of the Fe, which we obtain from hydrodynamics code simulations.
- The VISAR diagnostic provides a measure of the material velocity history at the back (free) surface.
- Incorporating a model for plasticity kinetics into the hydrodynamics code simulations better represents the physical processes that occur during wave propagation from front to back in the Fe.
- Accounting for the plasticity kinetics in the simulations we obtain much better agreement with measured free-surface velocity histories, which

gives us confidence that we can accurately calculate the pressure history at the front (drive) surface.

Acknowledgments

The authors would like to acknowledge the many useful and enlightening discussions they had with Mukul Kumar of Lawrence Livermore National Laboratory that have enhanced their understanding of plasticity. They would also like to thank Steve Pollaine of Lawrence Livermore National Laboratory for his careful review of this work. This work was performed under the auspices of the U. S. Department of Energy by the University of California, Lawrence Livermore National Laboratory (LLNL) under Contract No. W-7405-Eng-48, and was partially funded by the Laboratory Directed Research and Development project # 06-ERD-027.

References

Barker, L. M., and Hollenbach, R. E., 1972. Laser interferometer for measuring high velocities of any reflecting surface. J. Appl. Phys. **43**, pp. 4669-4675.

Boehly, T. H., Craxton, R. S., Hinterman, T. H., Kelly, J. H., Kessler, T. J., Kumpan, S. A., Letzring, S. A., McCrory, R. L., Morse, S. F. B., Seka, W., Skupsky, S., Soures, J. M., and Verdon, C. P., 1995. The upgrade to the OMEGA laser system. Rev. Sci. Instrum. **66**, pp. 508-510.

Colvin, J. D., Legrand, M., Remington, B. A., Schurtz, G., and Weber, S. V., 2003. A model for instability growth in accelerated solid metals. J. Appl. Phys. **93**, pp. 5287-5301.

Colvin, J. D., and Kalantar, D. H., 2006. Scaling of pressure with intensity in laser-driven shocks and effects of hot x-ray preheat. In: Furnish, M. D., Elert, M., Russell, T. P., and White, C. T. (eds.) Proc. APS Conf. Shock Compression of Condensed Matter, Amer. Inst. Phys. **CP845**, pp. 1413-1416.

Gilman, J. J., 1965. Microdynamics of plastic flow at constant stress. J. Appl. Phys. **36**, pp. 2772-2777.

Hawreliak, J., *et al*., 2006. Analysis of the x-ray diffraction signal for the α–ε transition in shock-compressed iron: Simulation and experiment. Phys. Rev. B **74**, 184107.

Kalantar, D. H., *et al*., 2003. Multiple film-plane diagnostic for shocked lattice measurements. Rev. Sci. Instrum. **74**, pp. 1929-1934.

Kalantar, D. H., *et al*., 2005. Direct observation of the α–ε transition in shock-compressed iron via nanosecond x-ray diffraction. Phys. Rev. Letters **95**, 075502.

Magnenet, V., Rahouadj, R, Ganghoffer, J.-F., and Cunat, C., 2007. Continuous symmetries and constitutive laws of dissipative materials within a thermodynamic framework of relaxation. Int. J. Plasticity **23**, pp. 87-113.

More, R. M., Warren, K. H., Young, D. A., and Zimmerman, G. B. 1988. A new quotidian equation of state (QEOS) for hot dense matter. Phys. Fluids **31**, pp. 3059-3078.

Remington, B. A., *et al*., 2004. Materials sceince under extreme conditions of pressure and strain rate. Metall. And Mat. Trans. A **35A**, pp. 2587-2607.

Smith, R. F., Eggert, J. H., Jankowski, A., Celliers, P. M., Edwards, J., Gupta, Y. M., Asay, J. R., Collins, G. W., 2006. Stiff response of aluminum under ultrafast shockless compression to 110 GPa. Phys. Rev. Letters **98**, 065701.

Steinberg, D. J. and Lund, C. M., 1989. A constitutive model for strain rates from 10^{-4} to 10^{6} s^{-1}. J. Appl. Phys. **65**, pp. 1528-1533.

Taylor, J. W. and Rice, M. H., 1963. Elastic-Plastic Properties of Iron. J. Appl. Phys. **34**, pp. 364-371.

Zel'dovich Ya. B. and Raizer, Yu. P., 2002. Physics of shock waves and high-temperature hydrodynamic phenomena. Dover Pub., Mineola, NY [Hayes, W. D. and Probstein, R. F., Eds.].

Zimmerman, G. B. and Kruer, W. L., 1975. Numerical simulation of laser-initiated fusion. Comments Plasma Phys. Controlled Fusion **2**, pp. 51-61.

Figure Captions

Fig. 1. a) Schematic of the three-layer target used in the laser-driven dynamic diffraction experiments. b) Fe free-surface velocity history as measured by the Visar diagnostic for one representative Omega laser shot with 117 J of beam energy, and as simulated without plasticity kinetics (blue curve).

Fig. 2. Schematic of the components of stress vs. strain in perfect plasticity with (red curve) and without (black curve) kinetics for uni-axial compression along the z axis.

Fig. 3. Pressure profiles in the Fe foil at the indicated times, as simulated without kinetics for the 117 J Omega laser shot.

Fig. 4. Fe free-surface velocity history as measured by the Visar diagnostic (black curve), as simulated without plasticity kinetics (blue curve), and as simulated with plasticity kinetics (red curve) for a) the 117 J Omega laser shot and the model parameters shown in column 2 of Table 1; b) the 117 J Omega laser shot and the model parameters shown in column 3 of Table 1; and c) the 179 J Omega laser shot and the model parameters shown in column 4 of Table 1.

Fig. 5. The Temperature-pressure trajectories of the front few microns of the Fe, as simulated with (red curve) and without (blue curve) plasticity kinetics, superposed on the temperature-pressure phase diagram for Fe.

Table 1. Model parameters used in the simulations

Parameter	Sim. 1	Sim. 2	Sim. 3
ρ_0 (cm^{-2})	10^6	10^6	10^6
M (cm^{-2})	10^{12}	10^{12}	10^{12}
D (GPa)	0.75	1.0	0.5
H (GPa)	0.2	0.2	0.2
Y_0 (GPa)	1.2	2.0 & 0.25	1.0

Notes:
Sim. 1 was for the 117 J Omega laser shot
Sim. 2 was for the 117 J Omega laser shot
Sim. 3 was for the 179 J Omega laser shot

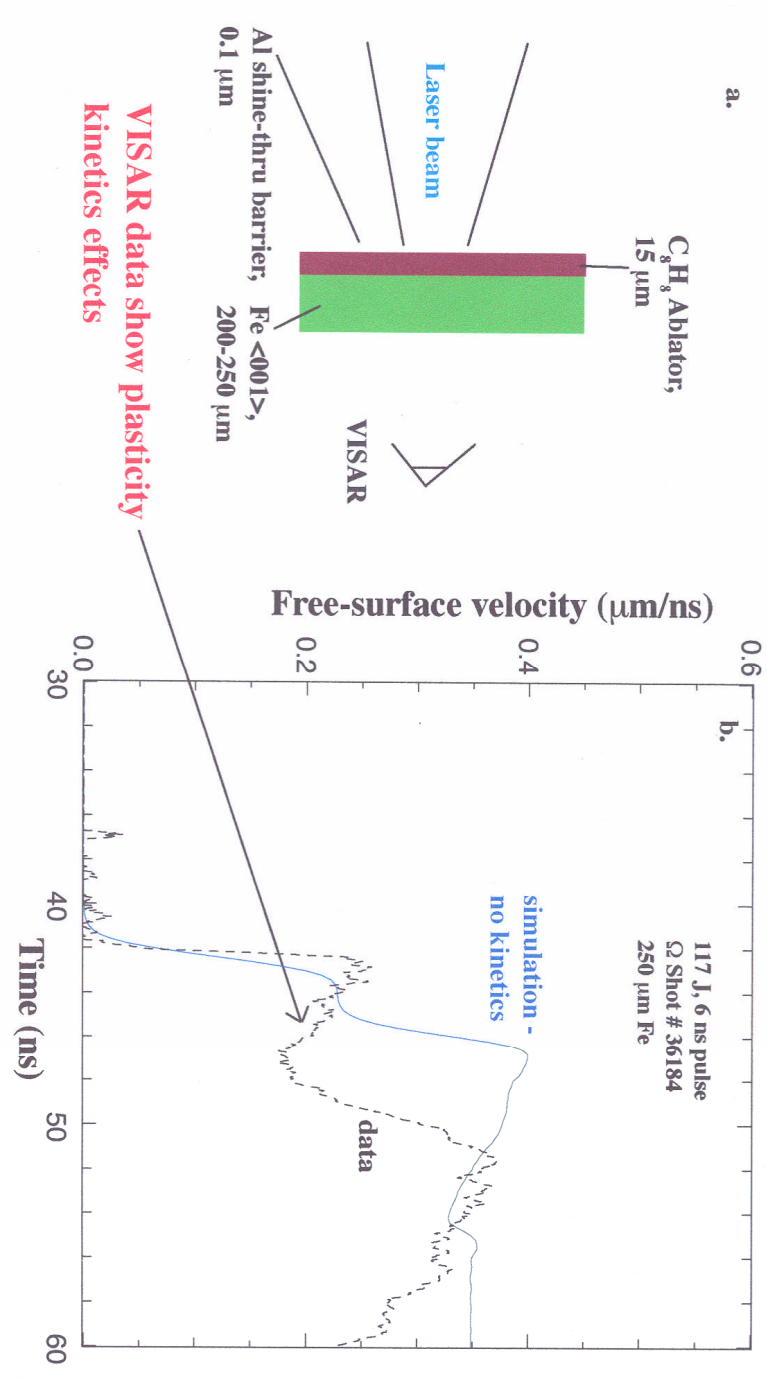
a.
Laser beam
C_8H_8 Ablator, 15 μm
Al shine-thru barrier, 0.1 μm
Fe <001>, 200-250 μm
VISAR
VISAR data show plasticity kinetics effects
b.
Free-surface velocity (μm/ns)
0.0
0.2
0.4
0.6
30
40
50
60
Time (ns)
117 J, 6 ns pulse
Ω Shot # 36184
250 μm Fe
simulation - no kinetics
data

Fig. 1

Fig. 2

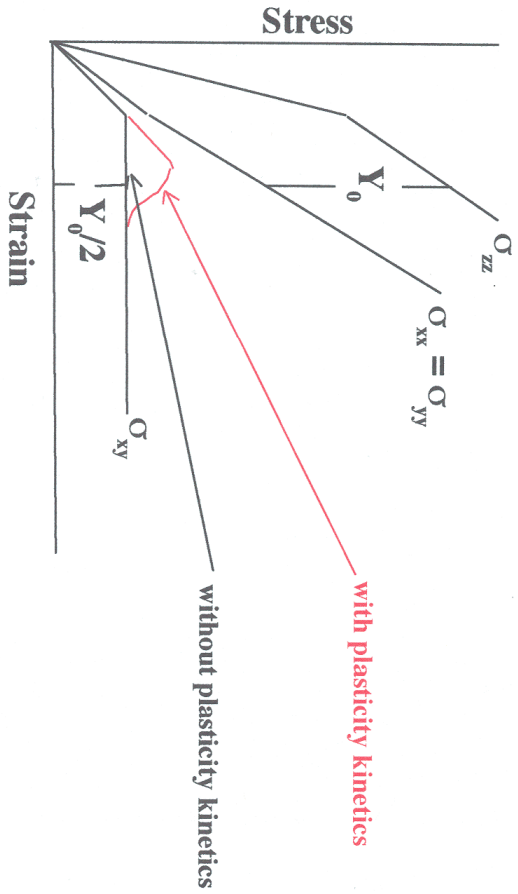
Stress
Strain
$Y_0/2$
Y_0
σ_{zz}
$\sigma_{xx} = \sigma_{yy}$
σ_{xy}
without plasticity kinetics
with plasticity kinetics

Fig. 3

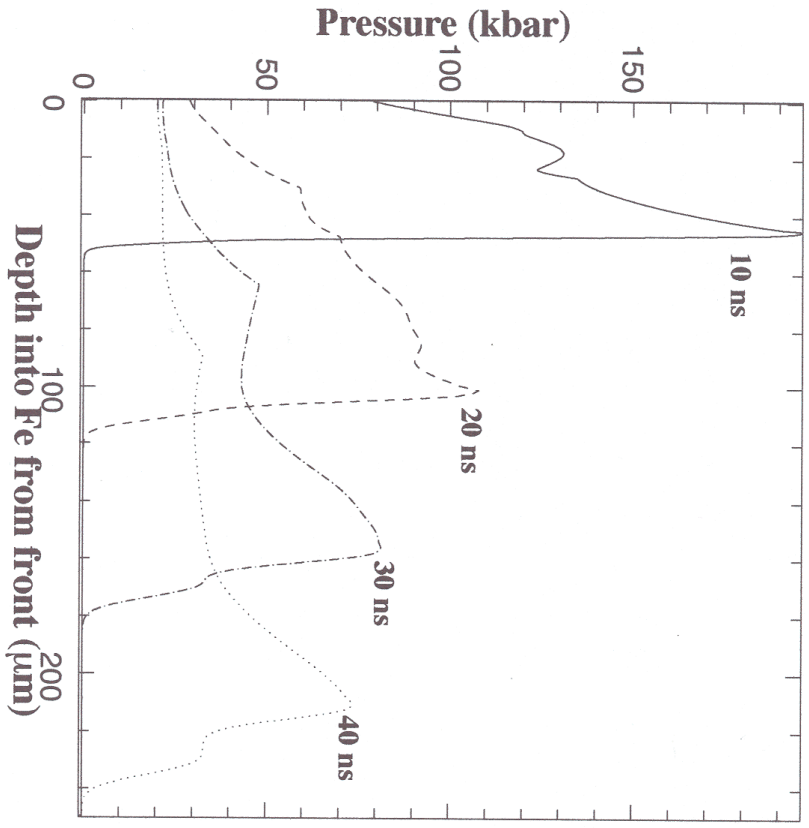
Pressure (kbar)
0
50
100
150
0
100
200
Depth into Fe from front (μm)
10 ns
20 ns
30 ns
40 ns

Fig. 4

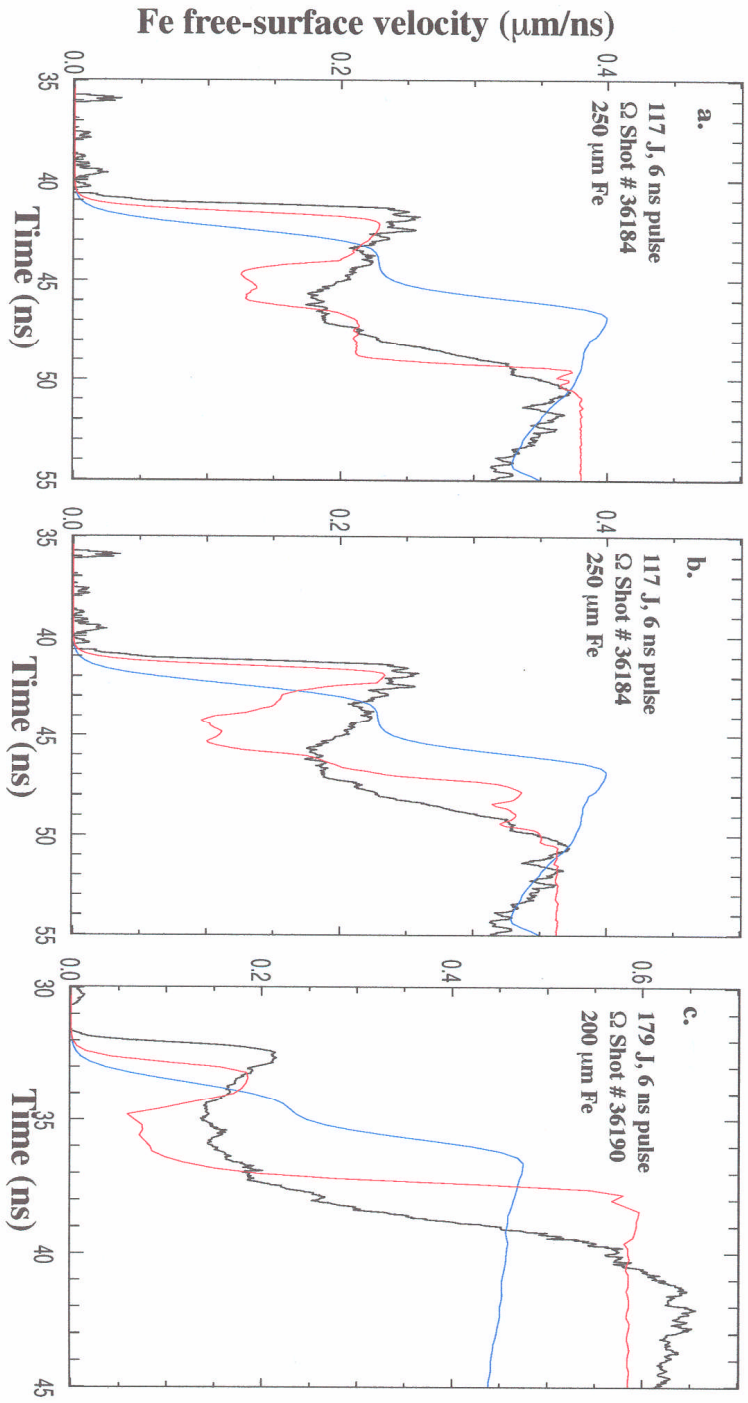
Fe free-surface velocity (μm/ns)
a.
117 J, 6 ns pulse
Ω Shot # 36184
250 μm Fe
b.
117 J, 6 ns pulse
Ω Shot # 36184
250 μm Fe
c.
179 J, 6 ns pulse
Ω Shot # 36190
200 μm Fe
Time (ns)

Fig. 5

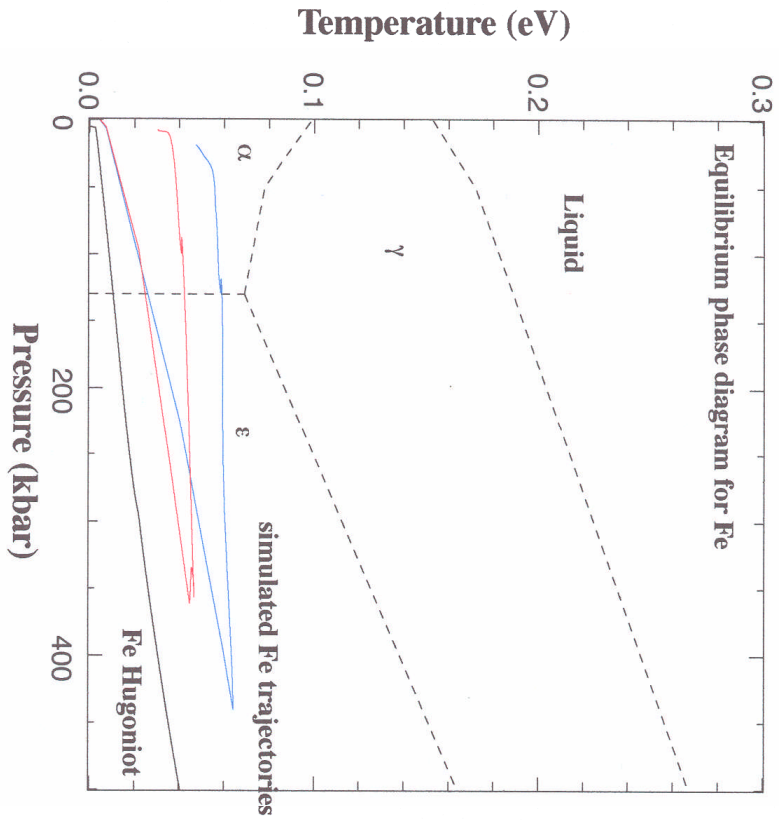
Temperature (eV)
0.0
0.1
0.2
0.3
Pressure (kbar)
0
200
400
Equilibrium phase diagram for Fe
Liquid
γ
α
ε
simulated Fe trajectories
Fe Hugoniot